^{18}F-FAC PET Visualizes Brain-Infiltrating Leukocytes in a Mouse Model of Multiple Sclerosis

Bao Ying Chen[1,2], Chiara Ghezzi[1,2], Brendon Villegas[3], Andrew Quon[1,4], Caius G. Radu[1,4], Owen N. Witte[1,5,6], and Peter M. Clark[1,2,5]

[1]Department of Molecular and Medical Pharmacology, UCLA, Los Angeles, California; [2]Crump Institute for Molecular Imaging, UCLA, Los Angeles, California; [3]Department of Pulmonary and Critical Care Medicine, UCLA, Los Angeles, California; [4]Ahmanson Translational Imaging Division, UCLA, Los Angeles, California; [5]Eli and Edythe Broad Center of Regenerative Medicine and Stem Cell Research, UCLA, Los Angeles, California; and [6]Department of Microbiology, Immunology, and Molecular Genetics, UCLA, Los Angeles, California

Brain-infiltrating leukocytes contribute to multiple sclerosis (MS) and autoimmune encephalomyelitis and likely play a role in traumatic brain injury, seizure, and stroke. Brain-infiltrating leukocytes are also primary targets for MS disease-modifying therapies. However, no method exists for noninvasively visualizing these cells in a living organism. 1-(2′-deoxy-2′-^{18}F-fluoroarabinofuranosyl) cytosine (^{18}F-FAC) is a PET radiotracer that measures deoxyribonucleoside salvage and accumulates preferentially in immune cells. We hypothesized that ^{18}F-FAC PET could noninvasively image brain-infiltrating leukocytes. **Methods:** Healthy mice were imaged with ^{18}F-FAC PET to quantify if this radiotracer crosses the blood–brain barrier (BBB). Experimental autoimmune encephalomyelitis (EAE) is a mouse disease model with brain-infiltrating leukocytes. To determine whether ^{18}F-FAC accumulates in brain-infiltrating leukocytes, EAE mice were analyzed with ^{18}F-FAC PET, digital autoradiography, and immunohistochemistry, and deoxyribonucleoside salvage activity in brain-infiltrating leukocytes was analyzed ex vivo. Fingolimod-treated EAE mice were imaged with ^{18}F-FAC PET to assess if this approach can monitor the effect of an immunomodulatory drug on brain-infiltrating leukocytes. PET scans of individuals injected with 2-chloro-2′-deoxy-2′-^{18}F-fluoro-9-β-D-arabinofuranosyl-adenine (^{18}F-CFA), a PET radiotracer that measures deoxyribonucleoside salvage in humans, were analyzed to evaluate whether ^{18}F-CFA crosses the human BBB. **Results:** ^{18}F-FAC accumulates in the healthy mouse brain at levels similar to ^{18}F-FAC in the blood (2.54 ± 0.2 and 3.04 ± 0.3 percentage injected dose per gram, respectively) indicating that ^{18}F-FAC crosses the BBB. EAE mice accumulate ^{18}F-FAC in the brain at 180% of the levels of control mice. Brain ^{18}F-FAC accumulation localizes to periventricular regions with significant leukocyte infiltration, and deoxyribonucleoside salvage activity is present at similar levels in brain-infiltrating T and innate immune cells. These data suggest that ^{18}F-FAC accumulates in brain-infiltrating leukocytes in this model. Fingolimod-treated EAE mice accumulate ^{18}F-FAC in the brain at 37% lower levels than control-treated EAE mice, demonstrating that ^{18}F-FAC PET can monitor therapeutic interventions in this mouse model. ^{18}F-CFA accumulates in the human brain at 15% of blood levels (0.08 ± 0.01 and 0.54 ± 0.07 SUV, respectively), indicating that ^{18}F-CFA does not cross the BBB in humans. **Conclusion:** ^{18}F-FAC PET can visualize brain-infiltrating leukocytes in a mouse MS model and can monitor the response of these cells to an immunomodulatory drug. Translating this strategy into humans will require exploring additional radiotracers.

Key Words: PET imaging; autoimmune disease; leukocytes; brain

J Nucl Med 2020; 61:757–763
DOI: 10.2967/jnumed.119.229351

Brain-infiltrating leukocytes drive pathology in multiple sclerosis (MS) and autoimmune encephalomyelitis (*1–4*). During MS, brain-infiltrating T cells, B cells, and macrophages promote neurodegeneration (*1–3*), and disease-modifying therapies modulate the immune system (*4*). Leukocytes are also found in the brains of murine models of traumatic brain injury, stroke, and seizure and of postmortem Parkinson disease and P301L tau frontotemporal dementia patients (*5–12*). Inhibiting leukocyte migration into the brain or depleting lymphocytes in these animal models can slow disease progression (*6–12*), suggesting a functional role for the immune system in these diseases. Although PET assays have been developed to image and quantify different aspects of neuroinflammation (*13–17*), there is no PET assay to visualize brain-infiltrating leukocytes. A noninvasive method to selectively image and quantify brain-infiltrating leukocytes would complement current approaches and provide information on the location of these cells during the development and treatment of neurologic diseases.

The radiotracer 1-(2′-deoxy-2′-^{18}F-fluoroarabinofuranosyl) cytosine (^{18}F-FAC) is a deoxyribonucleoside analog that measures deoxyribonucleoside salvage, a biochemical pathway enriched in leukocytes; accumulates at high levels in lymphoid tissues; and is increased in these same tissues in mouse models of immune activation (*18–20*). Additionally, ^{18}F-FAC accumulates at higher levels in activated T lymphocytes than in effector-memory T cells, CD11b-positive innate immune cells, or B220-positive B cells and at low levels in the healthy brain (*18–20*). Thus, we hypothesized that ^{18}F-FAC PET could noninvasively visualize brain-infiltrating leukocytes.

Here, we study ^{18}F-FAC in an experimental autoimmune encephalomyelitis (EAE) mouse model of MS. Our results suggest that ^{18}F-FAC PET can visualize brain-infiltrating leukocytes during disease and treatment.

MATERIALS AND METHODS

Mice

Ten-week-old female C57BL/6N and NOD.Cg-*Prkdc*^{scid} *Il2rg*^{tm1Wjl}/*SzJ* (NSG) mice were used for all experiments. All mouse experiments were approved by the UCLA Animal Resource Committee.

Received Apr. 2, 2019; revision accepted Oct. 7, 2019.
For correspondence or reprints contact: Peter M. Clark, Crump Institute, Box 951770, 4333 CNSI, Los Angeles, CA 90095-1770.
E-mail: pclark@mednet.ucla.edu
Guest Editor: Todd E. Peterson, Vanderbilt University
Published online Oct. 25, 2019.

Treatments

EAE treatments were conducted and scored similarly to a previously reported method (*15,21*). Briefly, mice were injected with an emulsion of myelin oligodendrocyte glycoprotein ($MOG_{35–55}$) in Freund complete adjuvant (100 μL) and with pertussis toxin (80 ng) at 2 h and again 24 h later (Hooke Laboratories). All experiments were conducted 13–15 d after immunization. Fingolimod (0.5 mg/kg; Selleckchem S5002) or vehicle was injected intraperitoneally daily starting immediately after immunization. Immunocompetent EAE mice were used at an average clinical score of 3.0.

Immunohistochemical Analyses

Sagittal brain sections (4 μm) were immunostained as previously described (*20*) except for the inclusion of CD45 (clone 30-F11; 1:100; Novus Biologicals), imaged at ×1 and ×40 magnification, and quantified using the Ilastik software (version 1.3.2). Boxes in the ×1 magnification images outline from where the ×40 magnification images were taken. To evaluate correlations, 2 independent ×40 magnification images were scored using an H-score (*22*).

^{18}F-FAC PET/CT

Mice that had been injected with either ^{18}F-FAC (1.85 MBq) or ^{18}F-FAC (1.85 MBq) and 10 mg of nonradiolabeled FAC were imaged for an hour or imaged 1 h after injection for 10 min on a G8 PET/CT device. The 1-h-postinjection time point was chosen as this is the earliest time point at which ^{18}F-FAC accumulation in the brain and blood no longer rapidly changes. Images were analyzed using AMIDE (version 1.0.4), and the magnetic resonance microimaging neurologic atlas was fitted to the mouse skull (*23,24*). Regions of interest were drawn at the interface of the hippocampus, thalamus, and midbrain as demarcated by the neurologic atlas. ^{18}F-FAC blood levels were determined from a region of interest drawn within the left ventricle of the heart.

^{18}F-CFA PET Analysis

^{18}F-CFA PET scans from a previous publication (*25*) were analyzed. Regions of interest were drawn similarly to those drawn on the mouse PET/CT images.

Ex Vivo Biodistribution Studies

Mice were injected with ^{18}F-FAC (1.85 MBq). One hour after injection, blood (100 μL) was collected, the mice were perfused, and organs were extracted and rinsed in ×1 phosphate-buffered saline. The activity and weight of the blood and organs were measured.

Autoradiography

Autoradiography was performed as previously described (*26*). Briefly, pre- and postimmunization EAE mice were injected with ^{18}F-FAC (18.5 MBq), and sagittal brain sections (10 μm) from perfused mice were cut.

Ex Vivo Accumulation Assays

Brain leukocyte isolation was conducted similarly to a previously description (*27*), and CD4-positive and CD11b-positive cells were isolated by fluorescence-activated cell sorting. Ex vivo deoxycytidine accumulation was performed as previously described (*20*) by incubating approximately 20,000 of each cell type in a 96-well filter plate with ^{3}H-deoxycytidine (0.037 MBq per well) for 30 min.

Statistical Analyses

Data were analyzed using GraphPad Prism (version 7.03). Statistical comparisons were performed using 2-sided *t* tests and 1-way ANOVA analyses with multiple comparison testing. Data are reported as mean ± SE

RESULTS

^{18}F-FAC Crosses the Healthy Blood–Brain Barrier (BBB) in Mice

To develop a PET assay to quantify brain-infiltrating leukocytes in neurologic diseases, we needed a PET radiotracer that accumulates in leukocytes and crosses the BBB. ^{18}F-FAC is a pyrimidine deoxyribonucleoside analog radiotracer that accumulates in leukocytes (*18,19*). Generally, pyrimidine ribonucleosides, except for uridine, do not cross the BBB, but studies suggest that ^{18}F-FAC accumulates at about 2 percentage injected dose (%ID)/g in the brain of healthy mice (*18,28*).

^{18}F-FAC accumulated at nearly uniform levels throughout the healthy mouse brain as evaluated by PET and autoradiography 1 h after injection (Figs. 1A and 1B). ^{18}F-FAC levels in the healthy mouse brain, corrected for blood volume in the brain (*29*), were slightly lower than ^{18}F-FAC levels in the blood (brain-to-blood ratio quantified from the PET images: 0.84 ± 0.05—brain: 2.54 ± 0.2 %ID/g, blood: 3.04 ± 0.3 %ID/g; brain-to-blood ratio quantified from isolated tissue and blood: 0.76 ± 0.05; Figs. 1C and 1D; ^{18}F-FAC time–activity curves are shown in Supplemental Fig. 1 (supplemental materials are available at http://jnm.snmjournals.org); correlation between brain-to-blood ratios quantified from the

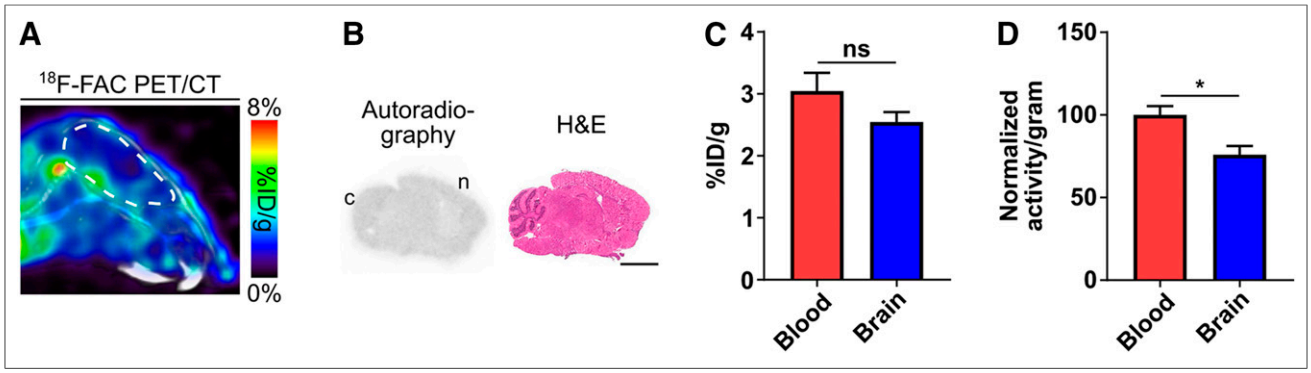

FIGURE 1. ^{18}F-FAC crosses the healthy BBB in mice. (A) Representative sagittal ^{18}F-FAC PET/CT image of a healthy C57BL/6 mouse. Brain is outlined in white. (B) Representative ^{18}F-FAC autoradiography and hematoxylin and eosin (H&E) staining of a sagittal brain section from a healthy C57BL/6 mouse. Scale bar = 3 mm; c = cerebellum; n = neocortex. (C) Blood and brain ^{18}F-FAC levels, quantified from PET images of healthy C57BL/6 mice (n = 5). (D) Normalized blood and brain ^{18}F-FAC levels, quantified from extracted blood and brain (n = 6). *P < 0.05. ns = not significant.

PET images and from isolated tissue and blood: $R^2 = 0.89$, Supplemental Fig. 2). ^{18}F-FAC has a logP value of −1.33, well below the 2–3.5 logP value of many radiotracers that diffuse into the brain and suggesting that ^{18}F-FAC is transported across the BBB (*30*). Collectively, these data suggest that ^{18}F-FAC crosses the healthy BBB.

Brain-Infiltrating Leukocytes Are Present in an EAE Mouse Model

EAE is a well-established MS model with leukocyte infiltration into the spinal cord and brain (*31,32*). EAE was induced in immunocompetent C57BL/6 and immunocompromised NSG mice by coinjecting $MOG_{35–55}$ in Freund complete adjuvant with pertussis toxin (*15,21*). Consistent with the literature (*15,21*), immunocompetent mice began to display EAE symptoms about 9 d after immunization that peaked about 13 d after immunization and included a limp tail, hind leg paralysis, and severe head tilting (Fig. 2A). Immunocompromised mice treated to induce EAE never displayed symptoms (Fig. 2A). Immunohistochemistry of immunocompetent mouse brain sections demonstrated significant perivascular and periventricular leukocyte infiltrates characterized by an abundance of CD11b-positive innate immune cells and CD4 T cells with few B220-positive B cells and CD8 T cells (Fig. 2B); 37% ± 2% of infiltrating leukocytes in these sections were dividing as suggested by Ki-67 immunostaining. No infiltrating leukocytes were observed in the immunocompromised EAE mouse brains (Fig. 2B). Isolated leukocytes from immunocompetent EAE mouse brains were similarly enriched for CD11b-positive innate immune cells and CD4 T cells (Fig. 2C).

^{18}F-FAC Accumulates at Higher Levels in the Brains of EAE Mice Than Control Mice

Immunocompetent and immunocompromised preimmunization and EAE mice were injected with ^{18}F-FAC and imaged by PET/CT 1 h later. ^{18}F-FAC accumulation in the brains of immunocompetent EAE mice was 180% of the levels of preimmunization immunocompetent

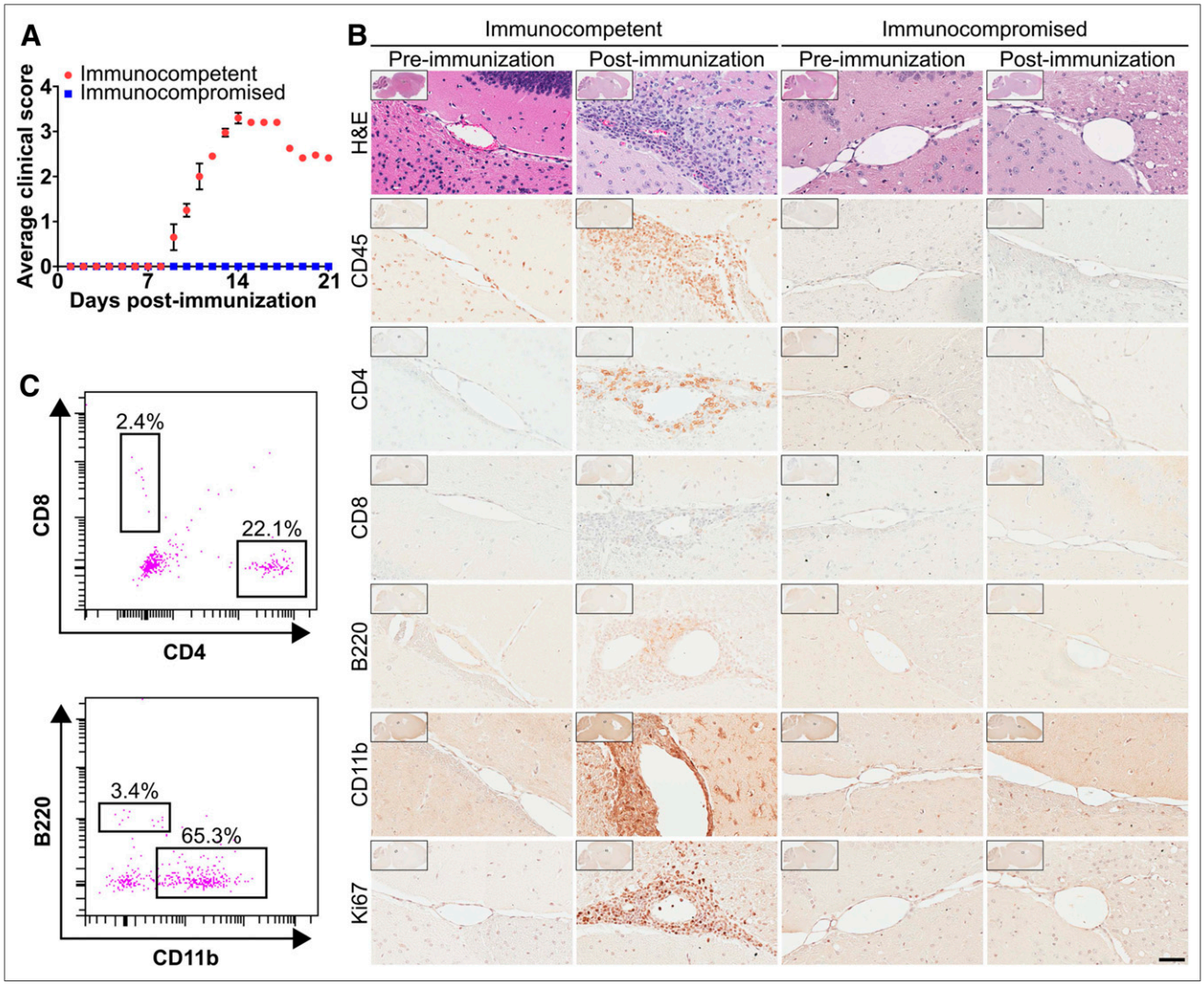

FIGURE 2. Brain-infiltrating leukocytes are present in a mouse model of EAE. (A) Time course of EAE symptoms in immunocompetent and immunocompromised mice ($n = 4$). (B) Hematoxylin and eosin and immunohistochemical stains of brain sections of mice before and after immunization. Images are at ×40 magnification, with ×1 shown in insets. Scale bar = 50 μm. (C) Immune cell populations isolated by fluorescence-activated cell sorting from immunocompetent EAE mouse brains ($n = 3$).

mice based on a region of interest drawn at the interface of the hippocampus, midbrain, and thalamus, where a high concentration of infiltrating leukocytes resides (preimmunization immunocompetent mice: 2.4 ± 0.15 %ID/g; immunocompetent EAE mice: 4.4 ± 0.66 %ID/g; Fig. 3A; Supplemental Fig. 3). ^{18}F-FAC accumulation in this same brain region of immunocompromised EAE mice was not significantly different from preimmunization immunocompromised mice (preimmunization immunocompromised mice: 3.2 ± 0.31 %ID/g; immunocompromised EAE mice: 2.4 ± 0.15 %ID/g; Fig. 3B; Supplemental Fig. 3). ^{18}F-FAC brain accumulation was lower in immunocompetent mice than in immunocompromised mice before immunization and was lower in postimmunization than in preimmunization immunocompromised mice. We cannot readily explain either of these results, although neither result reached statistical significance. ^{18}F-FAC accumulation was also significantly increased in the spleen and lymph nodes but not the femur, bone marrow, or spinal cord of the immunocompetent EAE compared with preimmunization mice (quantified from the PET images: spleen—preimmunization mice: 11.8 ± 2.1 %ID/g, EAE mice: 21.3 ± 3.2 %ID/g; lymph nodes—preimmunization mice: 2.3 ± 0.06 %ID/g, EAE mice: 9.1 ± 0.84 %ID/g; bone marrow—preimmunization mice: 14.7 ± 1.1 %ID/g, EAE mice: 11.9 ± 1.5 %ID/g; spinal cord—preimmunization mice: 4.9 ± 0.24 %ID/g, EAE mice: 5.7 ± 0.70 %ID/g; Supplemental Fig. 4; ex vivo biodistribution data are in Supplemental Fig. 5).

EAE mice have BBB breakdown, leading to the slow exchange or pooling of blood fluids in areas with significant leukocyte infiltration and a compromised BBB (*33*). Our results in the EAE model could be due to ^{18}F-FAC in these blood pools and not to specific cellular ^{18}F-FAC accumulation. Immunocompetent EAE mice were injected with ^{18}F-FAC supplemented with 10 mg of nonradiolabeled FAC. Cellular FAC accumulation can be saturated, but FAC accumulation in blood pools cannot. Coinjection of ^{18}F-FAC and nonradiolabeled FAC decreased brain ^{18}F-FAC accumulation in immunocompetent EAE mice by 57% compared with immunocompetent EAE mice injected with only ^{18}F-FAC and to 78% of the levels of preimmunization immunocompetent mice (preimmunization immunocompetent mice: 2.4 ± 0.15 %ID/g; immunocompetent EAE mice: 4.4 ± 0.66 %ID/g; immunocompetent EAE mice injected with ^{18}F-FAC and nonradiolabeled FAC: 1.9 ± 0.15 %ID/g; Fig. 3A; Supplemental Fig. 3). This suggests that the increased ^{18}F-FAC accumulation in the immunocompetent EAE mouse brains is due to specific cellular ^{18}F-FAC accumulation.

^{18}F-FAC Accumulates in Brain-Infiltrating Leukocytes in an EAE Mouse Model

Deoxycytidine kinase (dCK) phosphorylates ^{18}F-FAC and is a rate-limiting enzyme in the cellular accumulation of this radiotracer (*18,34*). Brain sections of preimmunization or EAE mice were immunostained with an antibody targeting dCK. Strong dCK immunostaining was apparent in 68% ± 5% of the infiltrating leukocytes in the brain sections of the immunocompetent EAE mice, and the intensity and number of immunostained leukocytes correlated with brain ^{18}F-FAC accumulation (R^2 = 0.85; Fig. 4A; Supplemental Fig. 6). In contrast, 37% ± 12% of leukocytes in the spinal cord of immunocompetent EAE mice, a tissue in which ^{18}F-FAC accumulation did not increase compared with preinjection mice, stained strongly for dCK (Supplemental Fig. 7). Weak dCK immunostaining was present in the brain parenchyma across all conditions, and the degree of dCK immunostaining in the brain parenchyma was unaffected by the EAE treatment (Fig. 4A). This suggests that increased brain ^{18}F-FAC accumulation in the immunocompetent EAE mice may be due to the tracer accumulating in the brain-infiltrating leukocytes. Consistent with this model, autoradiography of brain sections of immunocompetent EAE mice injected with ^{18}F-FAC shows the greatest enrichment in ^{18}F-FAC accumulation specifically in areas coincident with significant leukocyte infiltration in the EAE mouse brain (Fig. 4B).

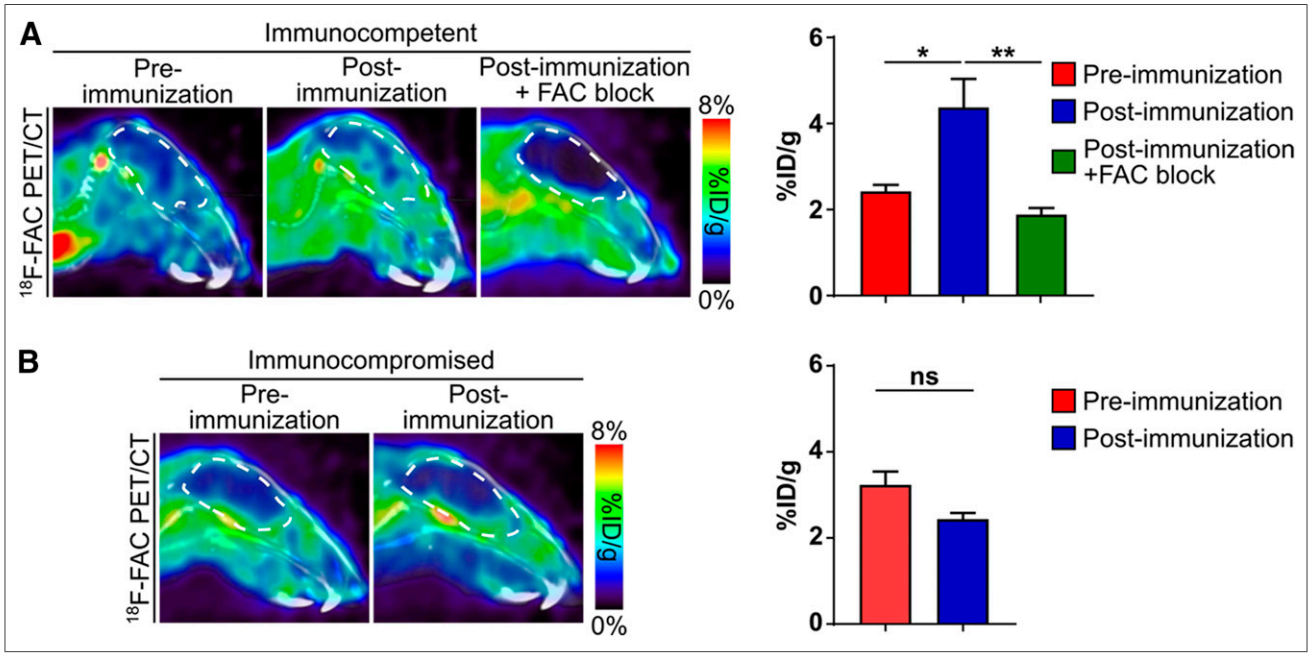

FIGURE 3. Brain accumulation of ^{18}F-FAC is higher in EAE mice than in control mice. Sagittal ^{18}F-FAC PET/CT images and quantification of immunocompetent (A) and immunocompromised (B) mice before and after immunization. Brains are outlined in white. FAC block = coinjection of mice with ^{18}F-FAC and nonradiolabeled FAC. n = 4 for all experiments. *P < 0.05. **P < 0.01. ns = not significant.

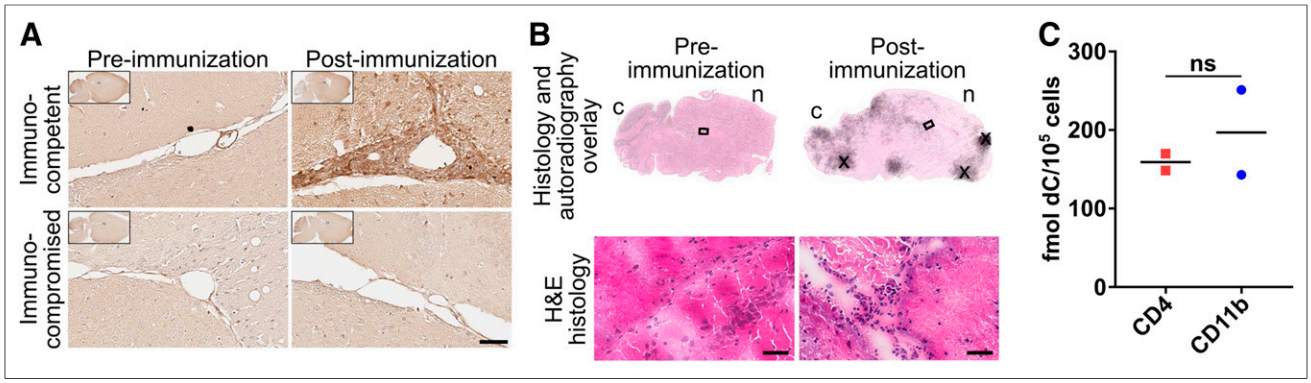

FIGURE 4. ^{18}F-FAC accumulates in brain-infiltrating leukocytes in an EAE mouse model. (A) dCK immunostaining of brain sections of mice before and after immunization. Images are at ×40 magnification, with ×1 shown in insets. Scale bar = 50 μm. (B) ^{18}F-FAC autoradiography images and hematoxylin and eosin staining of sagittal brain sections of immunocompetent mice before and after immunization. Images are at ×1 (top) and ×40 (bottom) magnification. Scale bar = 50 μm. c = cerebellum; n = neocortex; x = regions where tissue wrinkled. (C) Deoxycytidine (dC) accumulation in leukocyte populations isolated from immunocompetent EAE mouse brains (n = 2). ns = not significant.

Brain-infiltrating leukocytes in this model consist mostly of CD11b-positive innate immune cells and CD4 T cells (Figs. 2B and 2C). Deoxyribonucleoside salvage activity was similar between CD11b-positive innate immune cells and CD4 T cells isolated from the immunocompetent EAE mouse brains (Fig. 4C). Insufficient B220-positive B cells and CD8 T cells could be isolated for analysis. The number of leukocytes in the brain correlated with ^{18}F-FAC accumulation (R^2 = 0.82; Supplemental Fig. 8). Whether activated microglia also consume ^{18}F-FAC remains a topic for future study. However the overlap between the strong ^{18}F-FAC accumulation identified in the autoradiography and the areas identified by immunohistochemistry as having significant leukocyte infiltration (Figs. 2B and 4B) supports our interpretation that ^{18}F-FAC accumulates in—and that ^{18}F-FAC PET can image—brain-infiltrating leukocytes. Collectively, this suggests a model in which elevated ^{18}F-FAC accumulation in brain regions of immunocompetent EAE mice with significant leukocyte infiltration is due to ^{18}F-FAC accumulation in all of the brain-infiltrating leukocyte populations.

Changes in Brain ^{18}F-FAC Accumulation Can Monitor Immunomodulatory Drug Treatments in EAE Mice

The small-molecule fingolimod modulates the sphingosine-1-phosphate receptor, sequesters lymphocytes in lymph nodes and the spleen, and limits autoimmune diseases such as MS (*4,35*). Fingolimod decreased leukocytes in the brain of immunocompetent EAE mice compared with vehicle treatment (Fig. 5A). Fingolimod also significantly decreased brain ^{18}F-FAC accumulation compared with vehicle treatment in these same mice (pre-immunization mice: 2.0 ± 0.13 %ID/g, EAE mice treated with vehicle: 4.2 ± 0.25 %ID/g, EAE mice treated with fingolimod: 2.7 ± 0.08 %ID/g; Fig. 5B, Supplemental Fig. 3). Consistent with its mechanism of sequestering lymphocytes to lymph nodes and the spleen (*4,35*), fingolimod had no effect on ^{18}F-FAC accumulation in the lymph nodes and spleen of immunocompetent EAE mice (lymph nodes—EAE mice: 9.1 ± 0.84 %ID/g, EAE mice treated with fingolimod: 6.5 ± 0.26 %ID/g; spleen—EAE mice: 21.3 ± 3.2 %ID/g, EAE mice treated with fingolimod: 26.2 ± 1.8 %ID/g; Supplemental Figs. 3 and 4).

^{18}F-CFA Does Not Cross the BBB in Humans

^{18}F-FAC is deaminated in humans, but 2-chloro-2′-deoxy-2′-^{18}F-fluoro-9-β-D-arabinofuranosyl-adenine (^{18}F-CFA), a radiotracer that also measures deoxyribonucleoside salvage, is not (*36–38*). Accounting for blood volume in the brain (*39*), ^{18}F-CFA accumulates in the human brain at 11.0% ± 1.4% of the levels of ^{18}F-CFA found in the blood (135 min after injection: brain SUV: 0.08 ± 0.01; blood SUV: 0.54 ± 0.07; Supplemental Fig. 9), suggesting that ^{18}F-CFA does not cross the BBB in healthy human patients.

DISCUSSION

Despite studies showing that ^{18}F-FAC selectively accumulates in activated lymphocytes in mouse models of autoimmune hepatitis

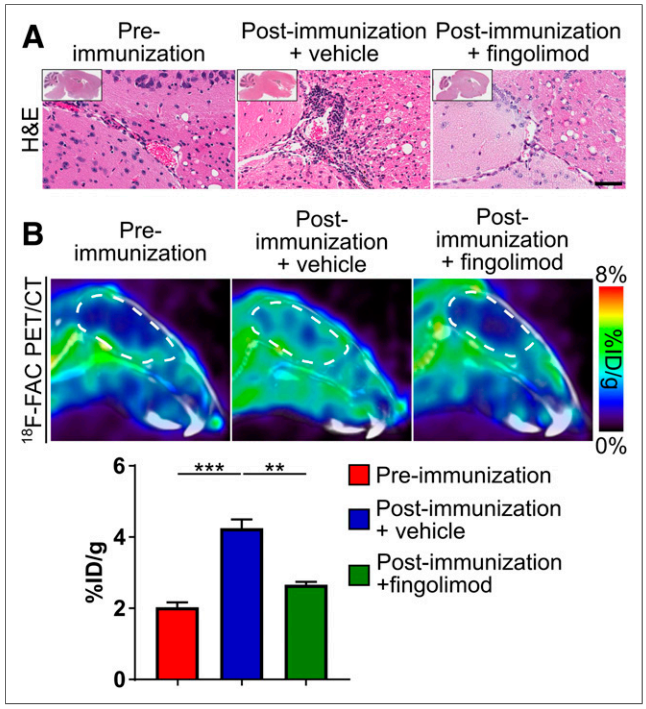

FIGURE 5. ^{18}F-FAC PET can monitor immunomodulatory drug treatments in an EAE mouse model. Hematoxylin and eosin stains of brain sections (A) and sagittal PET/CT images and quantification of ^{18}F-FAC accumulation (B) in brains of mice before and after immunization and treated with vehicle or fingolimod. Hematoxylin and eosin images are at ×40 magnification, with ×1 shown in insets. Brains are outlined in white. Scale bar = 50 μm. $^{**}P < 0.01$. $^{***}P < 0.001$.

and antitumor immunity (*18–20*), in the EAE mouse model we do not identify selective ^{18}F-FAC accumulation in brain-infiltrating lymphocytes. In the mouse model of antitumor immunity, the rate of ^{18}F-FAC accumulation in T cells was proportional to the rate of cellular proliferation (*19*). One explanation for our results is that brain-infiltrating lymphocytes are not rapidly dividing and thus do not consume high ^{18}F-FAC levels. Only 37% ± 2% of the brain-infiltrating leukocytes in our model are dividing, similar to the number of dividing liver-infiltrating leukocytes in a viral hepatitis model in which no enhanced hepatic ^{18}F-FAC accumulation was observed (*20*). ^{18}F-FAC is likely able to image infiltrating leukocytes in the EAE model but not the viral hepatitis model because of the approximately 50% lower basal accumulation of ^{18}F-FAC in the brain than the liver. ^{18}F-FAC may show selectivity for lymphocytes in other models with more actively dividing lymphocytes in the brain.

We show higher ^{18}F-FAC accumulation in brain-infiltrating leukocytes and in lymphoid organs such as the spleen and lymph nodes in the EAE model. ^{18}F-FAC measures deoxyribonucleoside salvage, for which dCK is a rate-limiting enzyme, and genetic knockout of dCK in healthy mice leads to decreased lymphocyte levels (*18,34*). Small-molecule dCK inhibitors with in vivo efficacy have been developed (*40*). Our data may suggest that dCK inhibitors could limit disease in this model.

A previous study found that ^{18}F-FDG accumulation in the spinal cord increased by 200% compared with control mice in this exact EAE model at the exact time point we studied (*15*). We identify no significant increase in spinal cord ^{18}F-FAC accumulation in the EAE mice, suggesting that in this model, immune cells in the spinal cord increase glucose but not deoxyribonucleoside consumption. This result is supported by the lower percentage of leukocytes in the spinal cord relative to the brain of EAE mice that stain strongly for dCK. These data suggesting that immune cells at different anatomic locations have different metabolic needs are consistent with data showing a much larger increase in ^{18}F-FDG than ^{18}F-FAC consumption in the draining lymph nodes of a mouse rhabdomyosarcoma model (*19*).

Brain-infiltrating leukocytes contribute to neurologic diseases, and MS and possibly other neurologic diseases can be treated with immunomodulatory drugs (*1–9*). Many immunomodulatory drugs cause significant side effects, and in MS the primary effects of these drugs on the immune system are assessed indirectly with MRI and clinical evaluations (*41*). PET assays with radiotracers that measure deoxyribonucleoside salvage could directly monitor the effect of these drugs on brain-infiltrating leukocytes. We demonstrate how this might work with the drug fingolimod.

Both ^{18}F-FAC and ^{18}F-CFA measure deoxyribonucleoside salvage (*18,38*). ^{18}F-CFA works poorly in mice because of high plasma deoxycytidine levels but is resistant to deamination in humans (*37,38*). However ^{18}F-CFA does not cross the BBB in humans, suggesting that a different radiotracer will need to be tested in humans. These could include the ^{18}F-FAC derivatives L-^{18}F-FAC and 2′-deoxy-2′-^{18}F-fluoro-5-methyl-β-L-arabinofuranosylcytosine, which are resistant to deamination (*36*). Additional studies would have to be conducted with these radiotracers to determine whether they cross the human BBB.

CONCLUSION

This study suggests that ^{18}F-FAC PET can noninvasively image brain-infiltrating leukocytes and can function as a pharmacodynamic biomarker of drugs that modulate these cells in mice. However, PET tracers that measure deoxyribonucleoside salvage and cross the BBB in humans will need to be further explored. We and others have shown that PET with radiotracers that measure deoxyribonucleoside salvage can image the immune system at least preclinically in various autoimmune conditions (*18,20*). The consistent activation of deoxyribonucleoside salvage in all of these settings may suggest a larger role for inhibitors of this pathway and a universal strategy for monitoring therapeutic responses in autoimmune disease.

DISCLOSURE

This work was supported by the UCLA Eugene Cota Robles Fellowship (to Bao Ying Chen), NIH grant R21AI119916 (to Peter Clark), NIH grant R01NS112287 (to Peter Clark), Parker Institute for Cancer Immunotherapy grant 20163828 (to Owen Witte), and the Broad Stem Cell Research Center at UCLA. Owen Witte and Caius Radu are inventors on a patent held by the University of California Regents that discloses ^{18}F-FAC. No other potential conflict of interest relevant to this article was reported.

ACKNOWLEDGMENTS

We thank the Crump Cyclotron and Radiochemistry Technology Center, the Crump Institute Preclinical Imaging Technology Center, the Translational Pathology Core Laboratory, and the Center for AIDS Research Flow Cytometry Core Facility at UCLA. We thank Eva Koziolek for tail vein injections. We thank Ralph and Marjorie Crump for their generous gift to the Crump Institute for Molecular Imaging.

KEY POINTS

QUESTION: Can PET imaging with ^{18}F-FAC, which measures deoxyribonucleoside salvage, visualize brain-infiltrating leukocytes, a cell population that can contribute to neurologic disease pathology and may serve as an important therapeutic target?

PERTINENT FINDINGS: ^{18}F-FAC accumulates in the brains of a MS mouse model at 180% of the levels found in the brains of control mice, and ^{18}F-FAC accumulates in areas of significant leukocyte infiltration and at nearly equal levels in brain-infiltrating T cells and innate immune cells. ^{18}F-FAC accumulation in the brains of these mice decreases by 37% when they are treated with the immunomodulatory drug fingolimod, suggesting that changes in brain ^{18}F-FAC accumulation can monitor a therapy in this model.

IMPLICATIONS FOR PATIENT CARE: A PET assay with a radiotracer that measures the deoxyribonucleoside salvage pathway may image brain-infiltrating leukocytes in patients with neurologic disease and during therapeutic interventions.

REFERENCES

1. Compston A, Coles A. Multiple sclerosis. *Lancet.* 2008;372:1502–1517.
2. Dendrou CA, Fugger L, Friese MA. Immunopathology of multiple sclerosis. *Nat Rev Immunol.* 2015;15:545–558.
3. Traugott U, Reinherz EL, Raine CS. Multiple sclerosis: distribution of T cell subsets within active chronic lesions. *Science.* 1983;219:308–310.
4. Wingerchuk DM, Carter JL. Multiple sclerosis: current and emerging disease-modifying therapies and treatment strategies. *Mayo Clin Proc.* 2014;89:225–240.
5. Bai R, Gao H, Han Z, et al. Long-term kinetics of immunologic components and neurological deficits in rats following repetitive mild traumatic brain injury. *Med Sci Monit.* 2017;23:1707–1718.

6. Ertürk A, Mentz S, Stout EE, et al. Interfering with the chronic immune response rescues chronic degeneration after traumatic brain injury. *J Neurosci.* 2016;36: 9962–9975.
7. Brochard V, Combadière B, Prigent A, et al. Infiltration of CD4+ lymphocytes into the brain contributes to neurodegeneration in a mouse model of Parkinson disease. *J Clin Invest.* 2009;119:182–192.
8. Laurent C, Dorothée G, Hunot S, et al. Hippocampal T cell infiltration promotes neuroinflammation and cognitive decline in a mouse model of tauopathy. *Brain.* 2017;140:184–200.
9. Dong T, Zhi L, Bhayana B, Wu MX. Cortisol-induced immune suppression by a blockade of lymphocyte egress in traumatic brain injury. *J Neuroinflammation.* 2016;13:197.
10. Yilmaz G, Arumugam TV, Stokes KY, Granger DN. Role of T lymphocytes and interferon-gamma in ischemic stroke. *Circulation.* 2006;113:2105–2112.
11. Grønberg NV, Johansen FF, Kristiansen U, Hasseldam H. Leukocyte infiltration in experimental stroke. *J Neuroinflammation.* 2013;10:115.
12. Varvel NH, Neher JJ, Bosch A, et al. Infiltrating monocytes promote brain inflammation and exacerbate neuronal damage after status epilepticus. *Proc Natl Acad Sci USA.* 2016;113:E5665–E5674.
13. Airas L, Dickens AM, Elo P, et al. In vivo PET imaging demonstrates diminished microglial activation after fingolimod treatment in an animal model of multiple sclerosis. *J Nucl Med.* 2015;56:305–310.
14. Unterrainer M, Mahler C, Vomacka L, et al. TSPO PET with [^{18}F]GE-180 sensitively detects focal neuroinflammation in patients with relapsing-remitting multiple sclerosis. *Eur J Nucl Med Mol Imaging.* 2018;45:1423–1431.
15. Radu CG, Shu CJ, Shelly SM, Phelps ME, Witte ON. Positron emission tomography with computed tomography imaging of neuroinflammation in experimental autoimmune encephalomyelitis. *Proc Natl Acad Sci USA.* 2007;104: 1937–1942.
16. James ML, Hoehne A, Mayer AT, et al. Imaging B cells in a mouse model of multiple sclerosis using ^{64}Cu-rituximab PET. *J Nucl Med.* 2017;58:1845–1851.
17. Gerwien H, Hermann S, Zhang X, et al. Imaging matrix metalloproteinase activity in multiple sclerosis as a specific marker of leukocyte penetration of the blood-brain barrier. *Sci Transl Med.* 2016;8:364ra152.
18. Radu CG, Shu CJ, Nair-Gill E, et al. Molecular imaging of lymphoid organs and immune activation by positron emission tomography with a new [^{18}F]-labeled 2′-deoxycytidine analog. *Nat Med.* 2008;14:783–788.
19. Nair-Gill E, Wiltzius SM, Wei XX, et al. PET probes for distinct metabolic pathways have different cell specificities during immune responses in mice. *J Clin Invest.* 2010;120:2005–2015.
20. Salas JR, Chen BY, Wong A, et al. ^{18}F-FAC PET selectively images liver-infiltrating CD4 and CD8 T cells in a mouse model of autoimmune hepatitis. *J Nucl Med.* 2018;59:1616–1623.
21. Miller SD, Karpus WJ. Experimental autoimmune encephalomyelitis in the mouse. *Curr Protoc Immunol.* 2007;77:15.1.1–15.1.18.
22. Fedchenko N, Reifenrath J. Different approaches for interpretation and reporting of immunohistochemistry analysis results in the bone tissue: a review. *Diagn Pathol.* 2014;9:221.
23. Loening AM, Gambhir SS. AMIDE: a free software tool for multimodality medical image analysis. *Mol Imaging.* 2003;2:131–137.
24. Ma Y, Hof PR, Grant SC, et al. A three-dimensional digital atlas database of the adult C57BL/6J mouse brain by magnetic resonance microscopy. *Neuroscience.* 2005;135:1203–1215.
25. Barrio MJ, Spick C, Radu CG, et al. Human biodistribution and radiation dosimetry of ^{18}F-clofarabine, a PET probe targeting the deoxyribonucleoside salvage pathway. *J Nucl Med.* 2017;58:374–378.
26. Salas JR, Chen BY, Wong A, et al. Noninvasive imaging of drug-induced liver injury with ^{18}F-DFA PET. *J Nucl Med.* 2018;59:1308–1315.
27. LaFrance-Corey RG, Howe CL. Isolation of brain-infiltrating leukocytes. *J Vis Exp.* 2011;52:2747.
28. Cansev M. Uridine and cytidine in the brain: their transport and utilization. *Brain Res Rev.* 2006;52:389–397.
29. Dai H, Marbach P, Lemaire M, Hayes M, Elmquist WF. Distribution of STI-571 to the brain is limited by P-glycoprotein-mediated efflux. *J Pharmacol Exp Ther.* 2003;304:1085–1092.
30. Pike VW. PET radiotracers: crossing the blood-brain barrier and surviving metabolism. *Trends Pharmacol Sci.* 2009;30:431–440.
31. Schmitt C, Strazielle N, Ghersi-Egea J-F. Brain leukocyte infiltration initiated by peripheral inflammation or experimental autoimmune encephalomyelitis occurs through pathways connected to the CSF-filled compartments of the forebrain and midbrain. *J Neuroinflammation.* 2012;9:187.
32. Brown DA, Sawchenko PE. Time course and distribution of inflammatory and neurodegenerative events suggest structural bases for the pathogenesis of experimental autoimmune encephalomyelitis. *J Comp Neurol.* 2007;502:236–260.
33. Bennett J, Basivireddy J, Kollar A, et al. Blood-brain barrier disruption and enhanced vascular permeability in the multiple sclerosis model EAE. *J Neuroimmunol.* 2010;229:180–191.
34. Toy G, Austin WR, Liao H-I, et al. Requirement for deoxycytidine kinase in T and B lymphocyte development. *Proc Natl Acad Sci USA.* 2010;107:5551–5556.
35. Cohen JA, Chun J. Mechanisms of fingolimod's efficacy and adverse effects in multiple sclerosis. *Ann Neurol.* 2011;69:759–777.
36. Shu CJ, Campbell DO, Lee JT, et al. Novel PET probes specific for deoxycytidine kinase. *J Nucl Med.* 2010;51:1092–1098.
37. Schwarzenberg J, Radu CG, Benz M, et al. Human biodistribution and radiation dosimetry of novel PET probes targeting the deoxyribonucleoside salvage pathway. *Eur J Nucl Med Mol Imaging.* 2011;38:711–721.
38. Kim W, Le TM, Wei L, et al. [^{18}F]CFA as a clinically translatable probe for PET imaging of deoxycytidine kinase activity. *Proc Natl Acad Sci USA.* 2016;113: 4027–4032.
39. Engvall C, Ryding E, Wirestam R, et al. Human cerebral blood volume (CBV) measured by dynamic susceptibility contrast MRI and ^{99m}Tc-RBC SPECT. *J Neurosurg Anesthesiol.* 2008;20:41–44.
40. Murphy JM, Armijo AL, Nomme J, et al. Development of new deoxycytidine kinase inhibitors and noninvasive in vivo evaluation using positron emission tomography. *J Med Chem.* 2013;56:6696–6708.
41. Calabresi PA, Radue E-W, Goodin D, et al. Safety and efficacy of fingolimod in patients with relapsing-remitting multiple sclerosis (FREEDOMS II): a double-blind, randomised, placebo-controlled, phase 3 trial. *Lancet Neurol.* 2014;13: 545–556.